This article has been accepted for publication in a future issue of this journal, but has not been fully edited. Content may change prior to final publication. Citation information: DOI 10.1109/JSEN.2021.3098861, IEEE Sensors Journal

Earbud-Embedded Micro-Power mm-Sized Optical Sensor for Accurate Heart Beat Monitoring

Assim Boukhayma, Anthony Barison, Serj Haddad, Antonino Caizzone

***Abstract*— This work demonstrates that accurate hear beat monitoring, via photoplethysmography (PPG), can be performed at micro-power consumption level with an ear worn device. This is achieved thanks to the combination of a highly sensitive low power PPG chip, an optimal optical module, and an ergonomic design of the wearable device. The monolithic optical sensor is fabricated in a 180 nm CMOS image sensor (CIS) process and features an area of 1.5 mm by 1.5 mm only. It implements an array of pixels, newly designed for PPG, and reaching a quantum efficiency of 85 % up to 800 nm. The presented sensor consumes 60 μA at 122 Hz sampling frequency, including digital communication. The optical design optimization enables high signal-to-noise ratio (SNR) PPG signals with less than 10 μA average LED current. Heart beat monitoring, using the presented wearable device, is performed on 7 subjects and compared with a medical electrocardiogram (ECG). The earbud device correctly detects 98.47 % of the beats on a total of 72.21 hours of recordings. The inter-beat interval (IBI) estimation from these recordings features a mean absolute error (MAE) as low as 7.52 ms.**

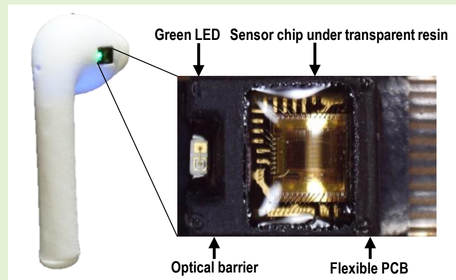

***Index Terms*— PPG, PPD, ultra-low-power, CMOS, Sensor, IBI, wearable.**

I. Introduction

Nowadays, efficient and remote health monitoring is becoming increasingly important, given both the ageing of population and the combined action of an increase in obesity level and cardiovascular diseases. The healthcare industry is becoming more reliant on new methods to monitor and treat patients. This, along with an increased interest in fitness and wellness, is calling for more affordable, precise and wearable health monitoring devices. In this context, photoplethysmography (PPG), also named optical heart sensing, appears to be a key technology allowing non-invasive monitoring of vital signs such as the heart rate, the blood oxygen saturation, the respiration rate and the arterial blood pressure [1].

A PPG signal is obtained by shining light from one or more LEDs at a given wavelength, from visible to near-infrared, into an human tissue, e.g. finger, wrist, ear lobs. As shown in Fig. 1, a photodetector (PD) detects the light transmitted through or reflected from the tissue and transforms it into a photogenerated current. The detected signal, i.e. PPG, consists of two different components: a large DC (quasi-static) component corresponding to the light diffusion through tissues and non-pulsatile blood layers, and a small AC (pulsatile) part due to the diffusion through the arterial blood. The AC component is only a very small fraction (typically 0.2% to 10%) of the DC one, depending on the body location and the skin tone [2]. For instance, at the same power, a wrist PPG exhibits a fairly lower AC than a finger one. The AC/DC ratio is called Perfusion-Index (PI) and represents one of the challenges of any PPG system in terms of dynamic range (DR) and power consumption [1], given that the majority of the medical information is carried by the tiny AC component.

The use of PPG sensors in wearables has been at first dominated by the smartwatches segment. Lately, the earbud segment is gaining the interest of most consumer wellness and health electronic devices manufacturers. The earbuds are very suitable for several use cases from fitness tracking to sleep monitoring. Moreover, the body location of the PPG sensor is an important issue affecting the signal quality or the sensor resilience to motion artifacts. In this regard, the ear is considered as one of the best locations in terms of PPG signals. It has been shown that the ear (particularly the canal area, both external and internal) features a PPG signal much less sensitive, than the limbs, to both motion-artifacts and perfusion changes induced by hypothermia [3], [4]. This leads to less power hungry operations and better vital signs extraction [5]. On the other hand, the ear location presents more challenges in terms of sensor integration and miniaturization.

State-of-the-art (SOA) PPG sensors, both in academia and in commercial products, still follow a quite standard design paradigm. Indeed, they rely on off-chip photodiodes and a relatively standard circuitry. The commercially available smartwatches and wearables often fall short of meeting

Authors are with Senbiosys SA, Neuchatel, Switzerland. e-mail: assim.boukhayma@senbiosys.com.

This article has been accepted for publication in a future issue of this journal, but has not been fully edited. Content may change prior to final publication. Citation information: DOI 10.1109/JSEN.2021.3098861, IEEE Sensors Journal

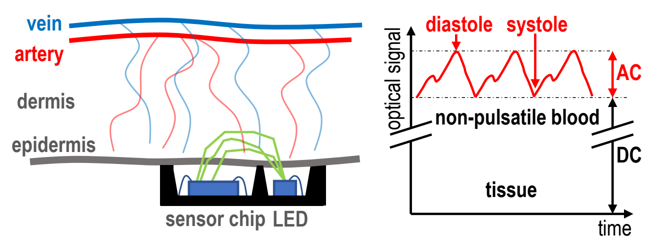

Fig. 1. Sensor set-up for a PPG measurement and the DC and AC components of a PPG signal.

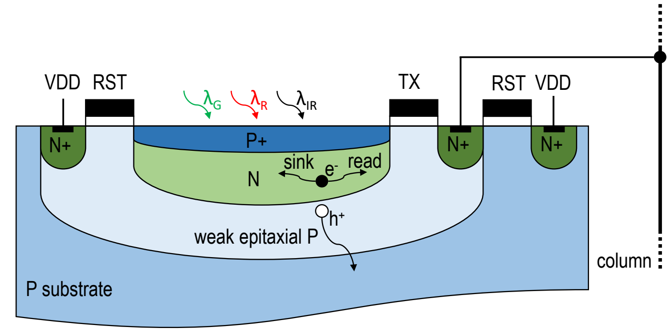

(a)

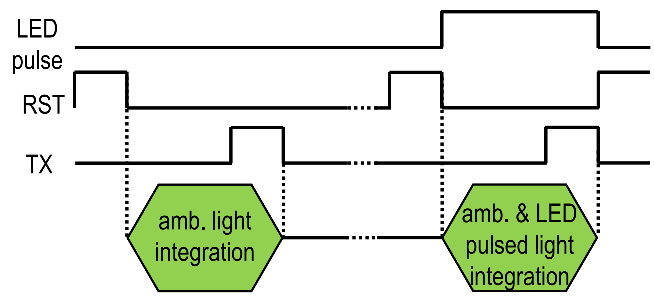

(b)

Fig. 2. The PPD-based pixel: (a) section diagram of the implemented pixel, (b) the timing diagram of the pixels and LED control.

customer requirements in terms of reliability, precision and battery lifetime. In this regard, we should not expect any dramatic improvement unless there are fundamental changes in the PPG sensor technology. This is particularly true on the photosensor side, since its parasitic capacitance represents one of the limiting factors in terms of power/noise [6].

Pinned-photodiodes (PPDs) are today the key ingredients of CMOS image sensors (CIS), thanks to the low dark current, low noise and large sensitivity operations [7], [8]. Several markets including security, scientific and medical imaging are relying today on this technology. The excellent performance of a PPD, demonstrated for different light sensing applications [9], makes it particularly interesting for the PPG application, as already presented in [10]–[12]. Indeed, the LED power can be reduced provided the noise floor is decreased proportionally.

Getting high fidelity PPG signals and good vitals extraction out of a high performance PPG sensor, integrated into a wearable device, requires optimization at different layers. First of all, no matter how good the PPG sensor is, in order to keep up the performance, this has to be integrated into an equally high-performance PPG module, the latter consisting of the PPG chip together with the LEDs. Placing those optical components together comes with several degrees of freedom and challenges too. At system level, the PPG module has to be integrated into the wearable device itself, in a manner which guarantees a good system management and as well ergonomics. Last, but not the least, the wearable device needs to provide accurate health data: in other words, the PPG module has to be paired with a solid algorithm.

This paper covers these different optimization layers in the case of an earbud and presents a multidisciplinary optimization leading to an accurate micro-power ear-worn PPG device. A newly designed sensor chip combining miniaturization with low power consumption and high sensitivity is presented. By integrating the latter in an optimized optical module, the LED current consumption required for high fidelity PPG signal is also reduced. Finally, it is demonstrated that the integration of this module into an ergonomic ear-worn device enables accurate heart beat detection in the ear, versus a medical device.

II. The micro-power mm-sized monolithic PPG Sensor

A. Sensor design

The presented monolithic PPG sensor is designed to cope with the following constraints: low area, low illumination, and low power consumption. Therefore, a specific pixel design featuring high quantum efficiency (QE) and large photo-electron density is required to cope with low LED light and small photosensitive area. At the same time, the monolithic integration of the pixels array together with a low-noise and low-power electronic allows enhanced miniaturization.

Fig. 2 shows a schematic view of the PPG-specific pixel together with the corresponding timing diagram. The pixel embeds a dual-tap PPD together with a reset gate. The PPD consists in a shallow heavily P-doped layer on top of a N-well that is placed in a lightly doped epitaxial layer [7], [13]. The doping concentration increases roughly by an order of magnitude between each two layers. Due to its vertical P+NP structure, the PPD features a potential well at the level of the N-doped region. The photo-electrons generated by the impinging photons accumulate at the level of the PPD potential well. The PPD device is connected to two gates (taps), one tap is used for dumping the integrated charge during reset, while the other tap is used to transfer the charge accumulated in the PPD well during the integration time windows. The sense node (SN) of the pixel is directly connected to the column to perform charge binning during the readout. A reset is performed before each integration. This allows to empty the PPD well and, at the same time, to set the column at a high voltage in order to attract the electrons accumulated in the PPD well during the integration. The pixels can perform two consecutive light integrations during windows as short as 10 μs. This allows two ambient light resilience mechanisms. The first is based on the short integration time and the second on the double sampling scheme that allows cancellation of the residual light. The pixel

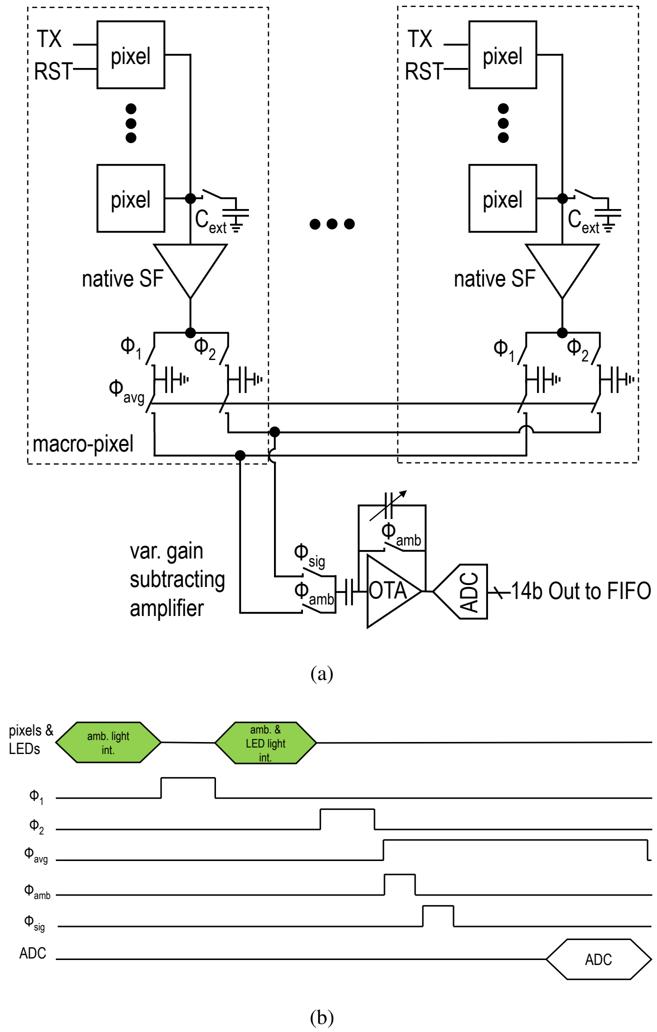

Fig. 3. (a) A block diagram of the sensor depicting the macro-pixels array, the subtracting amplifier and ADC, and (b) corresponding timing diagram.

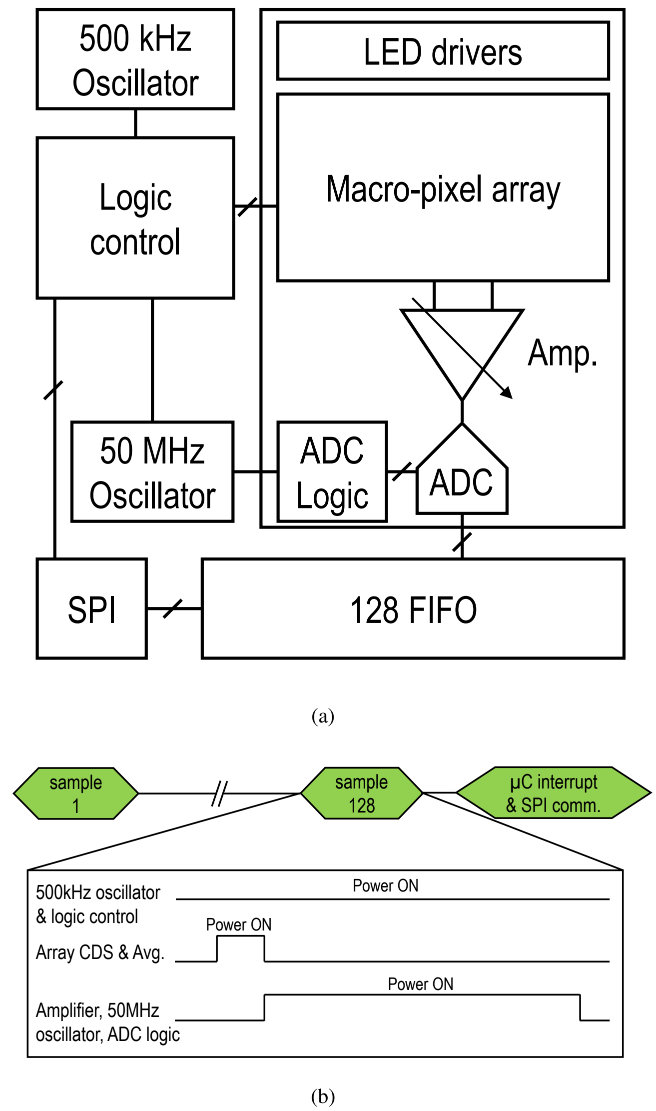

Fig. 4. (a) A block diagram of the sensor chip system design depicting the main functional blocks, and (b) corresponding timing diagram depicting the power and clock gating mechanisms.

also offers an important advantage for power reduction, on the emitter side, from the QE perspective. Indeed, a higher sensitivity leads to a same signal-to-noise ratio (SNR) with less emitted light. The presented pixel QE is improved thanks to the introduction of a weakly doped epitaxial layer under the PPD well. This weekly doped layer enhances the depth of the PPD depleted area which results in increasing the survival probability of electron-hole pairs, especially the ones generated deeper in the silicon, corresponding mostly to the higher wavelengths photons.

As shown in Fig. 3, the pixels sharing the same column SN are embedded in macro-pixels (MPs). Each MP also encompasses a switchable excess capacitance that enhances the dynamic range and a native source follower (SF) stage, operated in weak inversion region to ensure low power operations. The SF converts the charge transferred from the PPD to the SN into a voltage. Two sample-and-hold capacitors at the output of the SF ensure a double sampling scheme: one sample for the ambient light transfer and the second for the LED-originating light superimposed on the ambient one as described earlier in Fig. 2. Both samples are then averaged over the whole array in order to mitigate the electronic noise generated by the active circuits of the MPs. Indeed, it has been shown in [1] that an array of PPDs guarantees an important noise and power optimization. The two averaged samples are then fed to a switched capacitor (SC) variable gain amplifier stage that subtracts the two samples and buffers the amplified difference to an incremental 14 bit ADC. The working principle of the ADC and SC amplifier are detailed in [12]. Fig. 3(b) reports the whole front-end timing diagram, from the light integration to the ADC.

The presented monolithic sensor chip is designed to cope with a dynamic range of 90 dB, in order to cope with the high DC component of the PPG signal. The pixels feature a well density of $3 \cdot 10^5$ electrons/pixel. The number of photo-electrons necessary to reach 90 dB SNR is approximately $1.01376 \cdot 10^9$, hence the presented sensor features an array of 4096 pixels equally split between the 128 MPs. Regarding the readout chain, the native SFs stages ensure high dynamic since they

This article has been accepted for publication in a future issue of this journal, but has not been fully edited. Content may change prior to final publication. Citation information: DOI 10.1109/JSEN.2021.3098861, IEEE Sensors Journal

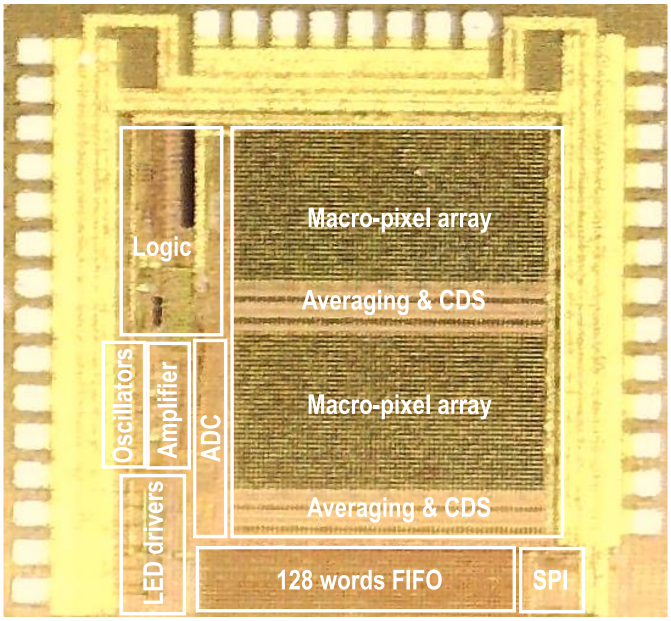

Fig. 5. Die micrograph showing the 1.5 mm by 1.5 mm sensor main building blocks integrated with pixels array.

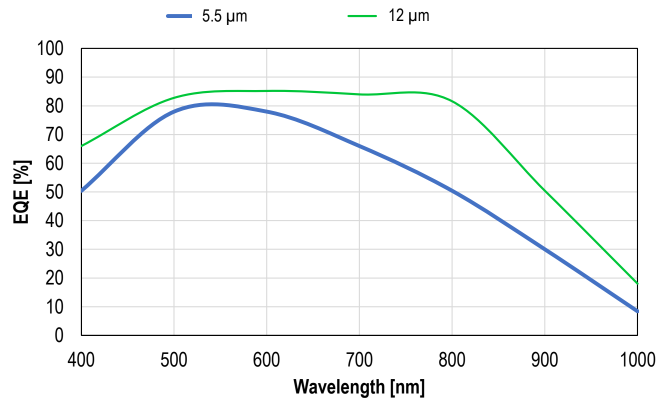

Fig. 6. Measured EQE of two versions of the PPD based pixel dedicated for PPG with two weakly doped epitaxial layer depth.

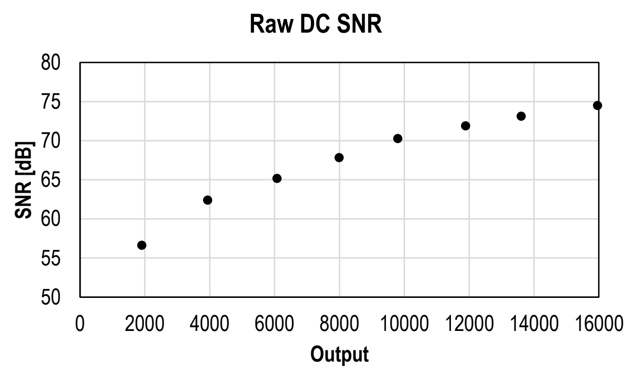

Fig. 7. Measured SNR as a function of the sensor output obtained by exposing the sensor to a varying input reflected DC light in loop-back mode.

feature a threshold voltage close to zero and hence an output swing of more than 2 V. At the level of the SN, the switchable capacitance C_{ext} allows to extend the dynamic in case the charge transferred to the SN induces a voltage drop exceeding 2 V. The amplifier is designed to feature a 2.5 V swing to preserve the dynamic range before the ADC.

The global architecture of the sensor analog readout chain is depicted in Fig. 4, together with the corresponding timing diagram. The chip also embeds, in addition to the pixels array and associated readout chain, LED drivers, embedded oscillators, digital control, 128 FIFO registers, and a serial peripheral interface (SPI) communication unit.

In order to optimize the power consumption at the circuit level, the sequential nature design of the readout chain is exploited extensively. As shown in Fig. 4(b), the array of SFs operating in weak inversion are disconnected from the power line once the ambient light and signal levels are stored in the MP capacitors. After that, the amplifier and ADC are powered only during the conversion. All of the chip blocks can operate with a slow clock of 500 kHz, except the incremental ADC that requires at least 50 MHz to obtain enough resolution in a reasonable time. Hence, the chip embeds two oscillators: a slow one consuming less than 2 μA and always on, and a second, oscillating at 50 MHz which is only turned on during the ADC operation. The digital design is also split in two blocks: one operating with the slow clock to ensure all of the chip functions and a sub-block operating with the fast clock only during the ADC operation. In this way, the chip power consumption is optimized taking advantage of both power and clock gating.

B. Sensor photo-electrical test

Fig. 5 shows a micrograph picture of the dedicated monolithic chip, specifically designed for ear PPG applications. The chip is fabricated in a 180 nm CIS process. The main blocks of the chip are highlighted in Fig. 5, namely, the dedicated pixels array, the amplifier, the ADC, the LED drivers, the embedded oscillators, digital control, 128 FIFO registers, and an SPI communication unit. Fig. 6 shows the measured QE of two pixel variants featuring two weak P type epitaxial layers depths. The proposed pixel features a weak P epitaxial depth of 12 μm, while the comparison pixel presented in [11], [12] features a 5 μm epitaxial layer. The weakly doped epitaxial layer role helps to deepen the depleted area of the PPD device. As already mentioned in Section II-A, this results in increasing the probability of electron-hole pairs generated deeper in the PPD to survive. This mechanism increases the QE especially towards near-infra-red (NIR) spectra, as shown by Fig. 6.

Fig. 7 shows the SNR, measured at the sensor output raw data (without digital filtering), in loop-back mode over the full DR of the sensor. This measurement is obtained by exposing the module, composed of the sensor and LEDs, to a stable reflector. The points of the curve are obtained by gradually increasing the LED driving current (set by the chip) and measuring the SNR for each LED driving configuration. In this way, this measurement of the SNR includes, not only the noise generated in the detection and readout process, but also the noise of the LED drivers and the LED themselves. The full system can go up to 75 dB without digital filtering. Since a PPG signal is very

TABLE I
SENSOR CHARACTERISTICS

Parameter	This work	[14]	[15]	[16]	[17]
Monolithic	yes	no	yes	no	no
Process	180 nm CIS	180 nm	65 nm CIS	180 nm	55 nm
Voltage supply	3.3/1.8 V	3.3/1.2 V	1.8/1 V	3.3/1.2 V	2.8/1.8 V
Area	2.25 mm^2	7 mm^2 excluding PD	5.5 mm^2	8.37 mm^2 excluding PD	4.5 mm^2 excluding PD
Integrated FIFO and SPI/I2C	yes (128 words)	no	yes (64 words)	no	yes with 16 kB memory
Max. sampling frequency	500 Hz	2048 Hz	20 Hz	2048 Hz	20 Hz
Max. dynamic range	90 dB	119 dB	90 dB	134 dB	130 dB
ADC resolution	14 bit	14 bit	16 bit	10 bit	14 bit
DR enhancement technique	extra SN capacitance	7 bit DC cancellation	High ADC resolution	7 bit DC cancellation and noise shaping	11 bit DC cancellation
Dynamic ambient light rejection	84 dB @ 1 Hz with 20 dB per decade decrease	not reported	46 dB below 120 Hz	not reported	not reported
Consumption	60 μA @ 122 Hz including digital	74 μA @ 522 Hz excluding digital	24 μA @ 20 Hz including digital	28 μW	72 μW

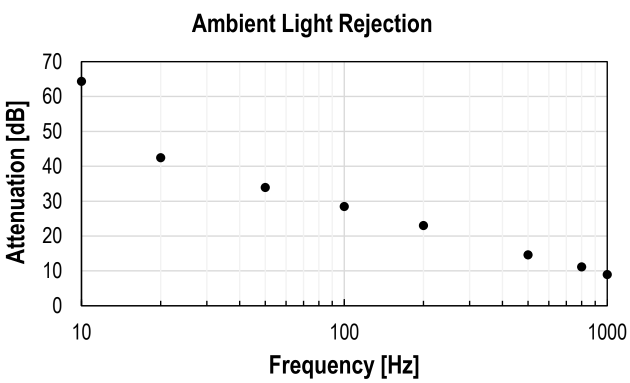

Fig. 8. Dynamic ambient light attenuation measurement.

often digitally filtered during the processing, the maximum SNR increases to 85 dB after band limiting the signal between 0.1 Hz and 4 Hz, thanks to a second order Butterworth filter. The maximum SNR is obtained when pixel array accumulates a minimum of 64 million photo-electrons, corresponding to an input photo-current of 115 nA for an integration window of 100 μs.

Ambient light resilience is an important characteristic of PPG sensors. The ambient light attenuation of the presented sensor is measured for both static and dynamic light. The measurement setup consists of placing the sensor in a dark chamber directly exposed to a wide band light emitter. The emitter is set to an intensity that reaches the saturation level of the sensor when the ambient light cancellation mode of the sensor is disabled. The attenuation is measured then as the sensor output when the ambient light cancellation is activated, normalized to the sensor maximum output. When operating the emitter in DC mode, the sensor cancels completely the ambient light. When the emitter is modulated at 1 Hz, an attenuation of 84 dB is reached. Fig. 8 shows the measured attenuation, when the emitter is modulated up to 1 kHz. The attenuation decreases following a 20 dB per decade slope, starting with 65 dB at 10 Hz.

Tab. I shows a summary of the main chip characteristics and performance metrics in comparison with recent SOA. The introduced chip presents a monolithic solution that stands out in terms of silicon area, power consumption and ambient light rejection, while embedding a 128 FIFO register and SPI communication protocol. The presented chip exhibits a relatively lower DR with respect to [14], [16], [17]. Over 120 dB DR is achieved in the reported literature thanks to a feedback loop subtracting a DC current component from the PD node at the input of the readout chain. Such a DC cancellation mechanism can certainly increase the DR, but also shows weakness with respect to dynamic ambient light. Indeed, against a fast ambient light variation, the DC cancellation loop might not react fast enough, leading to saturation. Large DR is particularly needed for PPG in body locations featuring low PI such as chest or forehead. The presented chip is rather targeting the ear concha or tragus, that feature a PI usually higher than 1%. Hence 90 dB dynamic is considered large enough for such application, especially that, for ear PPG, the LED illumination must stay as low as possible in order to remain invisible (for green light) and cope with the power consumption strict constraints. However, the proposed readout scheme can also be complemented by two DR enhancement techniques. The first consists of switchable extra capacitances at the SN. The second consists of performing a series of short exposures instead of a single one as shown in Fig. 2 and averaging the outputs in the same way the spatial averaging is performed. Successive short exposure can prevent the PPD and SN from saturation in case of large input light.

III. OPTICAL MODULE OPTIMIZATION

The optimization of a PPG module addresses several physical domains, such as optics, mechanics, electronics, and biology. In this section, the optimization of the opto-mechanical coupling between the PPG system and the skin is studied by simulating the effect of the distance between the LED and the PD array in terms of PI, SNR and optical power.

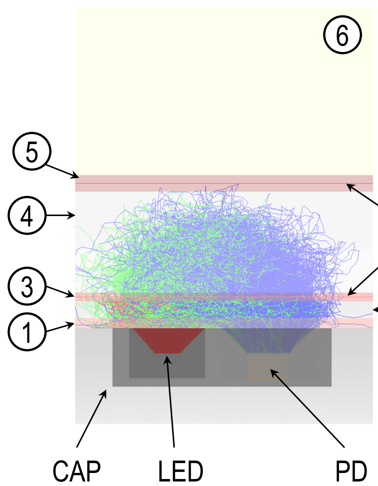

No.	Material	Thick. [μm]	Refr. Index	Absorption [1/mm]	*Anisotropy (g)	*Scatter Coeff. [1/mm]
1	Epidermis	120	1.335	0.5 @ 530 nm 0.26 @ 660 nm	0.8 @ 530 nm 0.8 @ 660 nm	31.3 @ 530 nm 22.1 @ 660 nm
2	Papillary dermis	200	1.37	0.28 @ 530 nm 0.15 @ 660 nm	0.8 @ 530 nm 0.8 @ 660 nm	19.2 @ 530 nm 14.4 @ 660 nm
3	Plexus superficialis	100	1.4	1.20 @ 530 nm 0.33 @ 660 nm	0.78 @ 530 nm 0.82 @ 660 nm	21.9 @ 530 nm 19.2 @ 660 nm
4	Reticular dermis	1200	1.37	0.28 @ 530 nm 0.15 @ 660 nm	0.8 @ 530 nm 0.8 @ 660 nm	19.2 @ 530 nm 14.4 @ 660 nm
5	Plexus profundus	200	1.4	1.38 @ 530 nm 0.34 @ 660 nm	0.78 @ 530 nm 0.82 @ 660 nm	22.5 @ 530 nm 19.4 @ 660 nm
6	Hypodermis	5000	1.44	0.28 @ 530 nm 0.4 @ 660 nm	0.8 @ 530 nm 0.8 @ 660 nm	16.3 @ 530 nm 12.3 @ 660 nm
7	Blood	Var.	1.335	180 @ 530 nm 1.88 @ 660 nm	0.8 @ 530 nm 0.8 @ 660 nm	701 @ 530 nm 894 @ 660 nm

* Henyey-Greenstein phase function.

Fig. 9. Skin model and optical parameters.

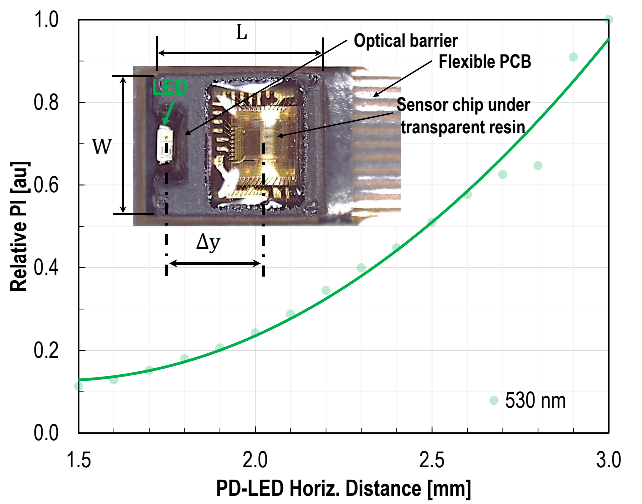

Fig. 10. Simulated relation between relative PI and PD-LED distance at 530 nm.

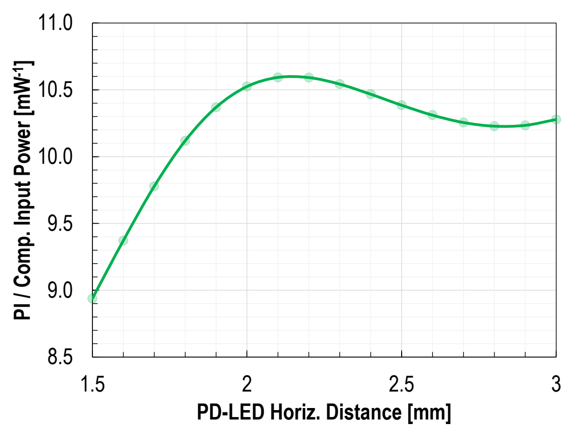

Fig. 12. Simulated relation between the PI normalized to the LED power and PD-LED distance with 530 nm illumination and a constant SNR.

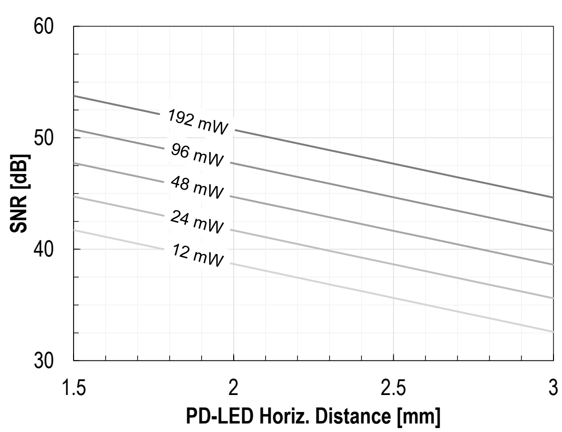

Fig. 11. Simulated relation between the SNR at the input of the sensor and PD-LED distance with 530 nm LED illumination.

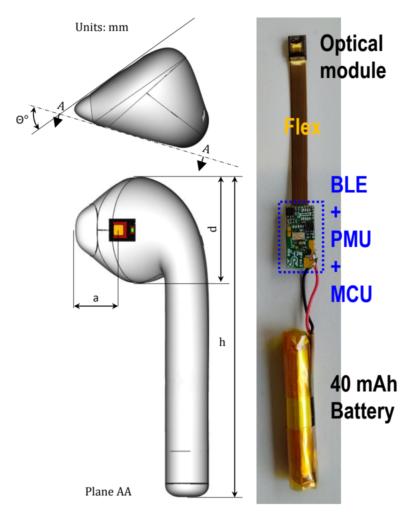

Fig. 13. Top and planar AA view of the earbud, including teardown of the electronic system.

Fig. 14. (a) Photograph of the ring device embedding the presented monolithic sensor and its optimized optical module, and, (b) Ear photographs with the target spots for PPG signal recording, namely, the tragus and concha.

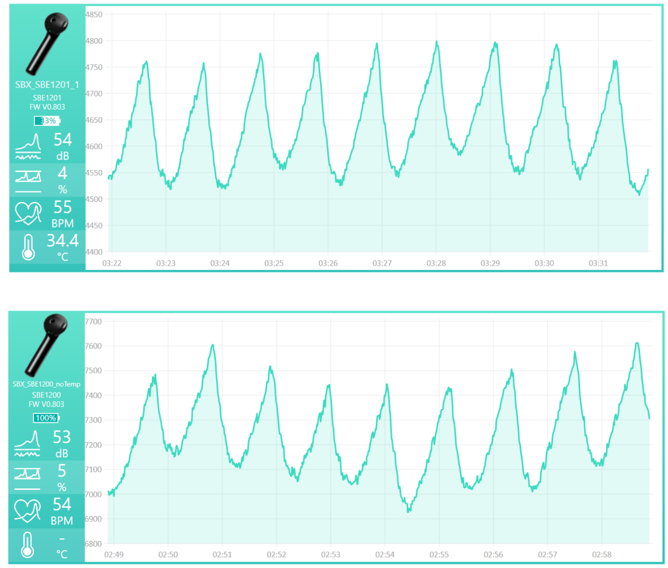

Fig. 15. PPG waveforms with high SNR recorded, on the same subject, using the presented earbud devices on the concha (a), and from the tragus (b).

As discussed in [1], a PPG signal consists of a large DC component and a small AC one imposed upon the former. The AC/DC ratio, namely PI, the lager the better, is the most important parameter around a PPG signal. First of all, a skin model was developed based on the literature. Histological studies, such as [18]–[22], finely describe the anatomical structure of the skin, in which three macro layers can be identified, namely the epidermis, the dermis and the hypodermis. The optical properties of the anatomical structure of the skin can be modeled by a seven layer structure, that was proven sufficient to model primary effects of photon-skin interaction, such as absorption and scattering [23]–[25]. Fig. 9 shows a cross-sectional cut-view of the simulated system consisting of a skin model, a simplified PPG system and the photon-path scattered through the skin. The optical properties and thickness of each layer were adapted from the literature, [20]–[22], [25]. It is worth noting that the statistical nature of such values is subject to laboratory procedures, sample preparation, origin of the sample. On the other hand, the ratio between epidermis and overall dermis as well as the percentage volume of blood for a given volume of dermis carries greater significance in understanding signal quality for a given optical flux. It is key, for whatever optical simulation intended to maximize the AC/DC ratio, to present a correct blood volume model, which ultimately accounts for its dynamic properties. In this regard, pulsatile component of blood volume was modeled as two homogeneous layers of oxygenated blood in the DPS and DPP regions having the following characteristics: a volumetric ratio of 1:2 and an overall volume of 0.6% (systole) and 0.2% (diastole) of the overall physical volume of dermis [26].
TracePro® and macro-scripting were used to combine Monte Carlo simulations and repetitive raytracing at differing blood volumes, while sweeping the distance between the centres of the PPG chip (PD) and LED. Fig. 10 shows the simulated relation between relative PI and PD-LED distance (Δy). The PI increases with the PD-LED distance. In agreement with the Beer-Lambert's Law, the DC component is found to decrease exponentially at a faster rate relative to the AC component.
The PPG signal SNR at the input of the optical sensor (PD) depends exclusively on the PI and the received optical power. Indeed, under the assumption that the shot noise is the dominant noise contributor and a low PI, the SNR can be approximated by $20log_{10}(PI \cdot \sqrt{N})$, where N is the number of detected photons. Fig.11 shows the simulated SNR as function of the LED-sensor distance for a given emitted optical power. As expected by the above SNR estimation, the simulation shows that even though the PI increases with the LED-sensor distance,

the SNR degrades due to the exponential decay of the number of received photons. Hence, from a pure SNR perspective, the LED-sensor distance must be kept as short as possible.

From a practical design aspect, a short LED-sensor distance also means small PI and hence very tight constraints on the dynamic range of the readout chain. A high dynamic readout chain requires large photo-electron capacity, high ADC resolution and tight noise constraints, which inevitably results in high power consumption and silicon area. In order to include the design complexity in our analysis, we define a figure-of-merit as the ratio between the PI and the optical power. Fig. 12 shows the simulated PI normalized to the optical power consumption for a constant SNR of 42 dB. This simulation shows that an optimum between the design complexity and optical power consumption exists at about 2.2 mm LED-sensor distance.

The optical simulations enable the optimization of the PPG module, consisting of the presented sensor and LED, shown in the inset of Fig. 10. The LED is an OSRAM CT DELSS1.12 with nominal wavelength at 530 nm. The module size $(W \cdot L \cdot H)$ is $3.2 \cdot 3.8 \cdot 0.6\,\mathrm{mm}^3$. The L dimension is ultimately set by the choice of the centre-to-centre distance between the PPD pixels array and the LED. We decided to place the LED at $\Delta y = 2.2\,\mathrm{mm}$ based on the above mentioned analysis.

IV. Earbud integration

The PPG module was embedded into an adhoc wearable earbud. The integration of the system faces a few challenges, namely, the miniaturization of the electronic system and the ergonomics. Fig. 13 shows top and planar AA view of the design, and a photo of the tear-down of the system showing the PPG module connected to the microcontroller unit and a set of custom-shaped batteries. The electronic system consists of the PPG module, a PCB hosting the microcontroller (MCU), power management unit (PMU) and low energy Bluetooth (BLE) and a 40 mAh cylindrical battery, 15 mm by 5 mm. The small form factor of the PPG module in Fig. 10 was beneficial in the positioning of the sensor to follow the curvature of the outer surface of the earbud shell. This resulted in having a continuous contact surface between the ear skin and the earbud. Secondly, the interconnection between the PCB and the PPG module was implemented with a FLEX board that provided some degrees of freedom in the mechanical integration. Finally, the size of the battery is found to be a trade-off between having an off-shelf part and a custom-shaped one, which directly affect the minimum size of the earbud. Referring to Fig. 13, the ergonomics of the earbud are primarily dependent upon the head diameter, d and the angle θ. These two parameters were set at 16.5 mm and 54° which allowed to fit all the population in our study, described in Section V. Secondly, the tail length is dependent upon the battery size and position of the PCB board within the earbud. According to previous experimental observations, the sensor location was found to be optimal at a equal to 6.75 mm, with respect to the AA plane. This was observed with respect to optimal PPG signal quality onto the tragus. The overall length of the earbud (h) is equal to 50 mm. Some functional prototypes, shown in Fig. 14, are 3D printed in stereolithography because of its intrinsic advantages, such as being cost-effective and having greater resolution for smaller features. A nylon-based material, EOS PA2200®, was selected because robust, flexible, stable for long periods of time and biocompatible under EN ISO 10993-1.

Fig. 14 shows two versions of the prototyped ear worn devices. One is targeting the PPG signal at the tragus of the ear and the second targets the PPG on the concha. Fig. 15 shows the PPG signal, measured on a same subject, using the tragus and concha prototypes. A fairly high SNR of 54 dB, on the raw data, is obtained at both ear locations while consuming only 70 μA at the optical module level (LED and sensor), at a sampling rate of 120 Hz. The prototype wearable earbud led to further ex-vivo studies of the PPG signal at the tragus and concha of the ear.

V. Heart beat monitoring performance

The ear-wearable system presented above relays on an optical module and monolithic sensor chip featuring low power and small form factor. In order to demonstrate that these advantages do not come at the cost of the PPG signal quality and its relevance for medical applications, a study performed on several subject is conducted to compare the precision of heart beat detection using the presented buds with a medical ECG.

A. Importance of accurate beat detection

Heart-rate variability (HRV), which is a physiological phenomenon that represents the change in the intervals of the consecutive heart-beats, is a very important index for the healthiness of the cardiovascular system. It is a measure of the cardiac activity that estimates the autonomous nervous system (ANS) balance [27]. As a matter of fact, HRV is closely associated with the overall physical fitness and the psychological well-being of an individual and it is used for stress and recovery analysis [27]. Since the outbreak of the COVID-19 pandemic the HRV data is becoming very crucial and is being heavily analyzed to study the effect of the COVID-19 on the mental health and the stress levels of individuals. HRV is also applied for sleep monitoring [28], and different types of arrhythmia detection [29], [30]. Therefore, it goes without saying that accurate, reliable, and continuous HRV monitoring is of utmost importance. An accurate HRV analysis, however, requires an efficient beat-to-beat heart rate detection [31], [32]. The classical method (the gold standard) of heart rate (HR) and HRV monitoring is using electrocardiography (ECG) devices. The drawback of the ECG recorders [33], [34] however is that they are highly uncomfortable and vulnerable to poor skin contact and dry skin conditions, which makes them unpleasant for long term recordings. As such, new solutions and methods that provide comfortable, unobtrusive, and inexpensive solutions are becoming highly attractive. Of these solutions and technologies, PPG is the most promising and favorable to provide low cost and agreeable alternative for HR and HRV monitoring.

B. Beat detection using the earbud

In what follows, we present a study that we performed to examine the beat-to-beat detection accuracy of using the PPG

TABLE II
THE STATISTICS OF THE REFERENCE RR INTERVALS.

Number of RRI's	213072
Mean $\pm$ SD (ms)	1040 ± 170
pNN50 (%)	29.40
pNN20 (%)	71.13

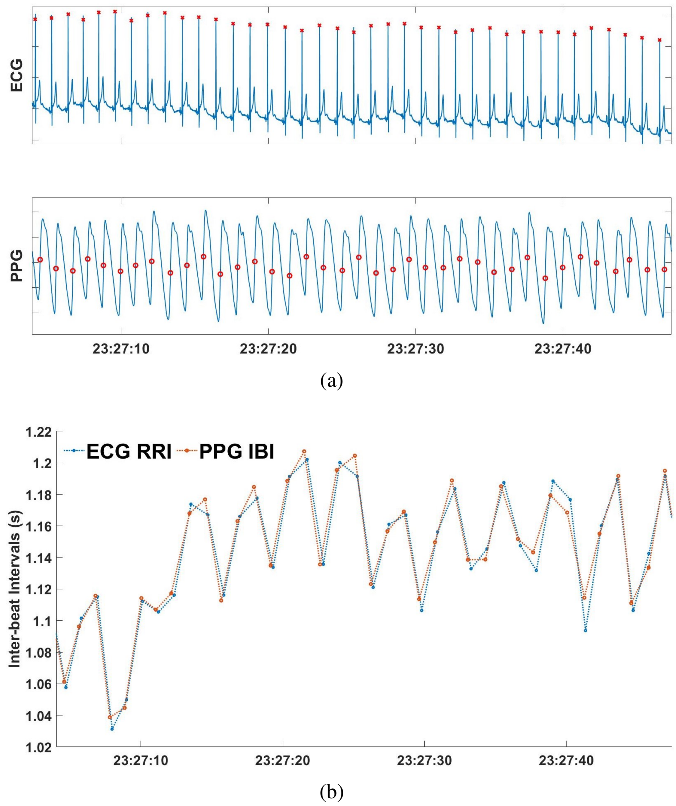

Fig. 16. (a) A plot of ECG and PPG signals with R-peak and maximum up-slope detection (red labels), respectively. (b) Corresponding ECG-based RR intervals and PPG-based IBI's.

signal recorded by the presented earbud. Seven male subjects with a mean age of 34.29 ± 5.28 years participate in the study. In total, 43 day and night recordings are performed with a total duration of 72.21 hours: 37.10 hours of *sleep* and 35.11 hours of *wake* recording. All *wake* recordings are done during working hours with as little motion as possible, while the *sleep* recordings are done during sleep. The participants are asked to wear the earbud in the left ear. Although we expected that the earbud gets displaced during the night recordings, it remained intact in all the recordings ensuring a good quality PPG signal. The sampling frequency of the earbud is set to 122 Hz and the driving current of the LED is set to 4.1 mA. For the reference ECG recordings, the Shimmer3 Consensys ECG development kit is used to monitor 4 ECG channels. The sampling frequency for the ECG recordings is set to 1024 Hz.

To extract the inter-beats interval (IBI) values from the PPG signals, we use the Senbiosys proprietary IBI detection software [35]. Note that the IBI detection and estimation algorithm is ran offline on the raw PPG data that is sent to the computer via bluetooth low energy (BLE). On the other hand, to extract the RR intervals (RRI) from the ECG signals, we use the ConsensysPRO Software version 1.6.0. In Fig. 16(a), we present plots of ECG and PPG recordings. The plots include (in red labels) the detection of R-peaks of the ECG signal and the detection of the maximum up-slopes of the PPG signal. These points are used to generate the ECG-based RR intervals and the PPG-based IBI values, depicted in Fig. 16(b). Further technical details regarding the algorithm can be found in [35].

In Table II, we summarize the statistics of the reference RRI values. The mean RRI value is 1.04 ± 0.17 s, which means that on average the participants have HR values less than < 60 beats per minute. Moreover, the average HRV of the participants can be considered to be fairly high with a pNN50 and pNN20[1] values of 29.40% and 71.13%, respectively.

TABLE III
THE BEAT DETECTION PERFORMANCE.

Correctly Detected Beats	209811
Correct Beats (%)	98.47
Missed Beats (%)	1.53
Extra Beats (%)	1.84

TABLE IV
THE PERFORMANCE OF THE IBI ESTIMATION.

MAE (ms)	7.52
ME (ms)	0.65
RMSE (ms)	13.71
MAPE (%)	0.74

C. Performance Evaluation

The performance of the IBI detection algorithm using the earbud is summarized in Table III. The classification of the beats as correct, missed, and extra beats is performed based on the technique proposed in [35]. We label each PPG beat as a correct beat, a missed beat, or an extra beat, based on the number of ECG beats detected in the vicinity of the PPG beat. We count the number of beats detected using the ECG signal in the interval $[t - 0.5l, t + 0.5l]$, where t is the time when the PPG beat was detected and l is the length of the corresponding IBI. If only one reference ECG beat is detected, then the corresponding PPG beat is labeled as a correct beat. If no reference beat is detected in the specified interval, then the corresponding PPG beat is labeled as an extra beat. All the ECG beats that are not referenced by a PPG beat are considered to be missed PPG beats. The results show that the percentage of the correctly detected beats is 98.47%. On the other hand, the percentage of the extra beats is only 1.84%.

For the IBI estimation, given that our recordings lack motion detection signals, such as triaxial acceleration signals, we use the following strategy to discard the noisy intervals. We divide

[1]pNN50 and pNN20 denote the percentage of the RR intervals with a successive difference exceeding 50 ms and 20 ms, respectively.

TABLE V
THE BEAT DETECTION-ESTIMATION PERFORMANCE: WAKE VS SLEEP.

	Wake	*Sleep*
Correct Beats (%)	97.49	99.21
Missed Beats (%)	2.51	0.79
Extra Beats (%)	2.68	1.21
MAE (ms)	8.23	7.01
ME (ms)	0.91	0.47
RMSE (ms)	16.14	12.00
MAPE (%)	0.77	0.72

the PPG recordings into 10-second intervals. Then, we keep the intervals where the algorithm correctly detects more than 80% of the reference beats. This is justified by the fact that intervals containing many missed or extra beats also contain, with high probability, motion artifacts. These artifacts may result not only from the mobility of the forearm, but also from very minor finger movements. For accurate IBI detection performance analysis and statistics computation, we therefore remove the intervals containing noisy signals. Upon discarding, 166275 beats are retained ($\sim$ 80% of the all the detected beats) for the IBI estimation. In Table IV, we summarize the IBI estimation accuracy of the PPG with a mean absolute error (MAE) of 7.52 ms, a mean error (ME) of 0.65 ms, a root mean square error (RMSE) of 13.71 ms, and a mean absolute percentage error (MAPE) of 0.74%. As shown in Table V, these beat detection and IBI estimation performance metrics improve for sleep/night recordings because of the absence of motion artifacts. The beat estimation performance obtained suggests the feasibility of performing HRV analysis using the proposed earbud.

VI. CONCLUSION

Continuous and accurate heart beat monitoring is achieved with the presented earbud while consuming only 60 μA at the chip level and less than 10 μA average LED current. This performance is obtained thanks to a multidisciplinary optimization. The device embeds a monolithic optical sensor exploiting CIS process and featuring 2.25 mm^2 silicon area, which is considerably smaller than state of the art PPG sensors. It encompasses dedicated pixels featuring an almost flat QE response on the whole visible range, while still exhibiting good NIR response. The dedicated pixels array is combined with low power design and CMOS integration to result into an ultra-low power and miniaturized sensor chip.

The advantages obtained thanks to the monolithic sensor integration are enhanced by an optimal optical module design maximizing the PI of the PPG signal. The latter is optimized thanks to optical simulations emulating how the LED light propagates in the human skin.

The performance is further enhanced by an ergonomic design of the earbud allowing better diffusion of the light through the ear skin on two possible ear positions, namely the tragus and the concha.

The earbud system exhibits high SNR PPG signal (over 50 dB) while consuming less than 70 μA on both sensor and emitter side. The two ear locations, tragus and the concha, show similar performance.

The system is validated for precise heart beat detection by comparing the earbud to a medical ECG device. The validation is performed on 7 subjects for a total of 72 hours of recording, distributed between wake and sleep time. 98.47 % of the beats are correctly detected versus an ECG gold standard and the IBI estimation from these recordings exhibits a MAE of 7.52 ms. This proposed wearable optical heart beat monitoring system shows a promising potential for wellness and medical health monitoring thanks to the ease of use, non-evasiveness and long battery life. Further clinical studies shall be performed to bring this wearable technology to the medical heath monitoring market. Future research can also focus on the comparison between the tragus and concha PPG on a larger population.

REFERENCES

[1] A. Caizzone, "An Ultra Low-Noise Micropower PPG Sensor," Ph.D. dissertation, EPFL, 2020.

[2] J. G. Webster, *Design of Pulse Oximeters*. Bristol, PA, USA: Philadelphia: Institute of Physics Pub., 1997.

[3] K. Budidha and P. Kyriacou, "Investigation of photoplethysmography and arterial blood oxygen saturation from the ear-canal and the finger under conditions of artificially induced hypothermia," in *Proceedings of the IEEE Annual International Conference of the Engineering in Medicine and Biology Society, EMBS*, Nov 2015, pp. 7954–7957.

[4] H. J. Davies, I. Williams, N. S. Peters, and D. P. Mandic, "In-ear spo2: A tool for wearable, unobtrusive monitoring of core blood oxygen saturation," *Sensors*, vol. 20, no. 17, 2020. [Online]. Available: https://www.mdpi.com/1424-8220/20/17/4879

[5] E. Tur, M. Tur, H. I. Maibach, and R. H. Guy, "Basal perfusion of the cutaneous microcirculation: Measurements as a function of anatomic position," *Journal of Investigative Dermatology*, vol. 81, no. 5, pp. 442 – 446, 1983. [Online]. Available: http://www.sciencedirect.com/science/article/pii/S0022202X15432312

[6] A. Caizzone, A. Boukhayma, and C. Enz, "Comprehensive Noise Analysis in PPG Read-out Chains," *2017 International Conference on Noise and Fluctuations (ICNF)*, pp. 1–4, June 2017.

[7] A. Boukhayma, *Ultra Low Noise CMOS Image Sensors*. Springer, 2018.

[8] A. Boukhayma, A. Peizerat, and C. Enz, "A sub-0.5 electron read noise vga image sensor in a standard cmos process," *IEEE Journal of Solid-State Circuits*, vol. 51, no. 9, pp. 2180–2191, Sep. 2016, DOI: 10.1109/JSSC.2016.2579643.

[9] A. Boukhayma, A. Caizzone, and C. Enz, "An ultra-low power ppg and mm-resolution tof ppd-based cmos chip towards all-in-one photonic sensors," *IEEE Sensors Journal*, vol. 19, no. 24, pp. 11 858–11 866, 2019.

[10] A. Boukhayma, A. Caizzone, and C. Enz, *Health monitoring device*. US patent US20200205680A1, 2017.

[11] A. Caizzone, A. Boukhayma, and C. Enz, "A 2.6μW Monolithic CMOS Photoplethysmographic Sensor Operating with 2μW LED Power," in *2019 IEEE International Solid- State Circuits Conference - (ISSCC)*, Feb 2019, DOI: 10.1109/ISSCC.2019.8662404, pp. 290–291.

[12] A. Caizzone, A. Boukhayma, and C. Enz, "A 2.6 μw monolithic cmos photoplethysmographic (ppg) sensor operating with 2 μw led power for continuous health monitoring," *IEEE Transactions on Biomedical Circuits and Systems*, vol. 13, no. 6, pp. 1243–1253, 2019.

[13] R. Capoccia, A. Boukhayma, F. Jazaeri, and C. Enz, "Compact modeling of charge transfer in pinned photodiodes for cmos image sensors," *IEEE Transactions on Electron Devices*, vol. 66, no. 1, pp. 160–168, Jan 2019, DOI: 10.1109/TED.2018.2875946.

[14] Q. Lin, J. Xu, S. Song, A. Breeschoten, M. Konijnenburg, C. Van Hoof, F. Tavernier, and N. Van Helleputte, "A 119db dynamic range charge counting light-to-digital converter for wearable ppg/nirs monitoring applications," *IEEE Transactions on Biomedical Circuits and Systems*, vol. 14, no. 4, pp. 800–810, 2020.

[15] S. j. Jung, J. Ryu, W. Kim, S. Lee, J. Kim, H. Park, T. Jang, H. Jeong, J. Kim, J. Park, R. Kim, J. Park, H. Jo, W. J. Kim, J. Yang, B. Sohn, Y. Han, I. Lim, S. Yoo, C. Park, D. g. Jang, B. H. Ko, J. Lim, J. Kim, K. Lee, J. Lee, Y. Park, and L. Yan, "A 400-to-1000nm 24 uw monolithic ppg sensor with 0.3a/w spectral responsivity for miniature wearables,"

in *2021 IEEE International Solid- State Circuits Conference (ISSCC)*, vol. 64, 2021, pp. 1–3.

[16] Q. Lin, S. Song, R. V. Wegberg, M. Konijnenburg, D. Biswas, C. V. Hoof, F. Tavernier, and N. V. Helleputte, "28.3 a 28μw 134db dr 2nd-order noise-shaping slope light-to-digital converter for chest ppg monitoring," in *2021 IEEE International Solid- State Circuits Conference (ISSCC)*, vol. 64, 2021, pp. 390–392.

[17] Y.-S. Shu, Z.-X. Chen, Y.-H. Lin, S.-H. Wu, W.-H. Huang, A. Y.-C. Chiou, C.-Y. Huang, H.-Y. Hsieh, F.-W. Liao, T.-F. Zou, and P. Chen, "26.1 a 4.5mm2 multimodal biosensing soc for ppg, ecg, bioz and gsr acquisition in consumer wearable devices," in *2020 IEEE International Solid- State Circuits Conference - (ISSCC)*, 2020, pp. 400–402.

[18] I. M. Braverman, "The cutaneous microcirculation: Ultrastructure and microanatomical organization," *Microcirculation*, vol. 4, no. 3, pp. 329–340, 1997.

[19] O. Arda, N. Göksügür, and Y. Tüzün, "Basic histological structure and functions of facial skin," *Clinics in Dermatology*, vol. 32, no. 1, pp. 3–13, 2014.

[20] K. Chopra, D. Calva, M. Sosin, K. K. Tadisina, A. Banda, C. De La Cruz, M. R. Chaudhry, T. Legesse, C. B. Drachenberg, P. N. Manson, and M. R. Christy, "A comprehensive examination of topographic thickness of skin in the human face," *Aesthetic Surgery Journal*, vol. 35, no. 8, pp. 1007–1013, 2015.

[21] K. F. Oltulu P, Ince B, Kokbudak N, Findik S, "Measurement of epidermis, dermis, and total skin thicknesses from six different body regions with a new ethical histometric technique," *Turkish Journal of Plastic Surgery*, vol. 26, pp. 56–61, 2018.

[22] R. Maiti, M. Duan, S. G. Danby, R. Lewis, S. J. Matcher, and M. J. Carré, "Morphological parametric mapping of 21 skin sites throughout the body using optical coherence tomography," *Journal of the Mechanical Behavior of Biomedical Materials*, vol. 102, no. April 2019, 2020.

[23] V. V. Tuchin, S. Utz, and I. Yaroslavsky, "Tissue optics, light distribution, and spectroscopy," *Optical Engineering - OPT ENG*, vol. 33, no. 10, pp. 3178–3188, 1994.

[24] Y. H. Kao, P. C. Chao, and C. L. Wey, "Design and Validation of a New PPG Module to Acquire High-Quality Physiological Signals for High-Accuracy Biomedical Sensing," *IEEE Journal of Selected Topics in Quantum Electronics*, vol. 25, no. 1, 2019.

[25] Y. H. Kao, P. C. Chao, Y. Hung, and C. L. Wey, "A new reflective PPG LED-PD sensor module for cuffless blood pressure measurement at wrist artery," *Proceedings of IEEE Sensors*, vol. 2017-Decem, pp. 1–3, 2017.

[26] T. Lister, P. A. Wright, and P. H. Chappell, "Optical properties of human skin," *Journal of Biomedical Optics*, vol. 17, no. 9, p. 0909011, 2012.

[27] J. Sztajzel, "Heart rate variability: a noninvasive electrocardiographic method to measure the autonomic nervous system," vol. 134(35-36). Swiss Med Wkly, 2004, pp. 514–522.

[28] T. Myllymäki, H. Rusko, H. Syväoja, T. Juuti, M.-L. Kinnunen, and H. Kyröläinen, "Effects of exercise intensity and duration of nocturnal hear rate variability and sleep quality," *European Journal of Applied Physiology*, vol. 122, pp. 801–809, 2012.

[29] S. Haddad, J. Harju, A. Tarniceriu, T. Halkola, J. Parak, I. Korhonen, A. Yli-Hankala, and A. Vehkaoja, "Ectopic beat-detection from wrist optical signals for sinus rhythm and atrial fibrillation subjects," in *XV Mediterranean Conference on Medical and Biological Engineering and Computing – MEDICON*, September 2019, pp. 150–158.

[30] A. Tarniceriu, V. Vuohelainen, S. Haddad, T. Halkola, J. Parak, J. Laurikka, and A. Vehkaoja, "Performance of wrist photoplethysmography in monitoring atrial fibrillation in post cardiac surgery patients," in *2019 Computing in Cardiology (CinC)*, 2019, pp. 1–4.

[31] U. R. Acharya, K. P. Joseph, N. Kannathal, C. M. Lim, and J. S. Suri, "Heart rate variability: a review," in *Medical & Biological Engineering & Computing*, vol. 44, 2006, pp. 1031–1051.

[32] M. Malik, "Heart rate variability," *European Heart Journal Trans. Neural Networks*, vol. 17, pp. 354–381, 1996.

[33] L. C. Vanderlei, R. A. Silva, C. M. Pastre, F. M. Azevedo, and F. M. Godoy, "Comparison of the polar s810i monitor and the ecg for the analysis of heart rate variability in the time and frequency domains," *Brazilian Journal of Medical and Biological Research*, vol. 41, pp. 854–859, October 2008.

[34] L. Porto and L. Junqueira, "Comparison of time-domain short-term heart interval variability analysis using a wrist-worn heart rate monitor and the conventional electrocardiogram," in *Pacing and Clinical Electrophysiology*, vol. 32, January 2009, pp. 43–51.

[35] S. Haddad, A. Boukhayma, and A. Caizzone, "Beat-to-beat detection accuracy using the ultra low power senbiosys ppg sensor," in *8th European Medical and Biological Engineering Conference (EMBEC 2020)*. Springer, 2020, pp. 178–188.

Assim Boukhayma was born in Rabat, Morocco, on February 5th, 1988. He received the Ph.D. degree from the Ecole Polytechnique Fédérale de Lausanne (EPFL), Lausanne, Switzerland, on the subject of Ultra Low Noise CMOS Image Sensors. He received the Springer thesis award in recognition for his PhD outstanding Research. He is currently founder and chief scientific officer at Senbiosys SA, Neuchatel, Switzerland, and a scientific advisor for EPFL.

From 2012 to 2016, he worked at Commissariat a l'Energie Atomique (CEA-LETI),Grenoble, France, in the frame of his PhD research. From 2016 to 2019, he worked as research team leader at the Integrated Circuits Laboratory, EPFL.

Anthony Barison received his M.Sc. in Biomedical Engineering from Swiss Federal Institute of Technology (ETH) Zürich, Zürich, Switzerland, in 2019. He received the 2013 IEEE UK and RI Communication Chapter Prize in merit of his work on mm-wave steerable antennas at University of Essex, Colchester, United Kingdom.

He is currently a System Engineer at Senbiosys SA, Neuchâtel, Switzerland. His research interests include skin optics and opto-mechanical integration of photoplethysmography systems in wearable devices.

Serj Haddad received the B.E. and the M.Sc. degrees in computer engineering from the Lebanese American University (LAU) in 2010 and 2012, respectively, and the Ph.D. degree in computer and communication sciences from the Ecole Polytechnique Federale de Lausanne (EPFL) in 2017. Currently, he is a research engineer at Senbiosys working on developing algorithms for optical signals. His research interests include biomedical signal processing, random matrices, free space optics, and network information theory.

Antonino Caizzone was born in Milazzo, Italy, on March 20th, 1991. He received the Ph.D. at the 'Ecole Polytechnique Fédérale de Lausanne (EPFL), under the supervision of Prof. Enz and Dr. Boukhayma, on the subject of ultra-low noise and low power sensors for healthcare. He is currently founder and chief technology officer at Senbiosys SA, Neuchatel, Switzerland.

Between 2012 and 2013 he worked in STMicroelectronics Italy as an intern on the design of analog electronics on plastic substrate. In 2014, he worked at Georgia Tech. (USA) as visiting researcher on the subject of energy harvesters.